Calibration of the Davis Xenon Detector

Caroline Paciaroni
Physics Department, University of California, Davis
Physics Department, California Polytechnic State University, San Luis Obispo

The nature of dark matter is one of the greatest unsolved problems in physics. Many scientists believe Weakly Interacting Massive Particles (WIMPs) may be the answer, yet as the WIMP stubbornly remains theoretical, physicists are forced to create more and more sensitive detectors to continue their search. The LUX-ZEPLIN, or LZ, experiment is the newest detector being developed to probe the lowest limits for the WIMP cross-section. Here at UC Davis, a small-scale xenon time projection chamber, called the Davis Xenon Detector (DAX), has been built as a test-bed for LZ technologies. However, in order to produce meaningful results, it is essential to fully calibrate DAX. The main result of my work this summer was the calibration of the photomultiplier tube in DAX, though additional time was spent improving the pulse classification software and preparing the system for energy calibration and future experiments.

Introduction

A. The Existence of Dark Matter

The existence of dark matter (DM) was first theorized when astronomical observations showed a disconnect between the expected density of the universe due to visible matter and the gravitational behavior of galaxies. The initial cause for alarm was when the measurement of galactic rotation curves for spiral galaxies was found to be inconsistent with gravitational theory. The behavior of our local solar system closely matches the predictions of Newtonian gravity; the closer planets' velocities are much greater than the velocities of those on the outer edges. However, this does not hold true when observing entire galaxies. In a stable, Keplerian orbit, the rotational velocity of an object should scale as $v(r) \propto \sqrt{M(r)/r}$, where $M(r)$ is the mass inside the orbit and r is the radius around the galaxy. However, observations showed the velocity is approximately constant out to the visible edge of our galaxy, which leads to the conclusion that there is some "dark halo" of matter, with a mass density $\rho \propto 1/r^2$, with $M(r) \propto r$. One galactic rotation curve for nearby galaxy M33 is shown in Figure 1, where it is clear that the visible matter cannot account for the observed data [1].

This observational inconsistency started the theory of DM, though there are many other sources of evidence for its existence. One of these sources is the existence of old galaxies, which could only have formed in the early universe if DM was present to allow for matter domination. Others sources include observations of the potential energies of clusters of galaxies, measurements of the anisotropy of the Cosmic Microwave Background (CMB), and the spatial distribution of galaxies. Originally, it was hypothesized that there must be as much DM as there is luminating matter. Now, it is thought to make up as much as 85% of the total mass in the universe [2].

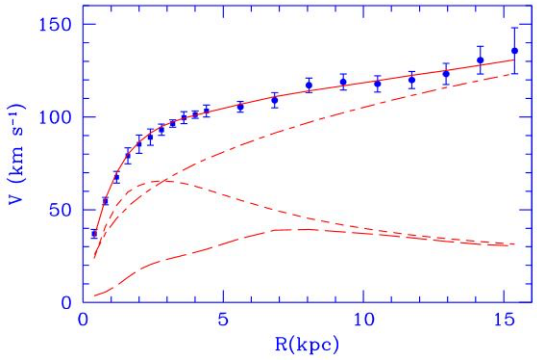

FIG. 1: Observed galactic velocity versus radius for nearby galaxy M33. The continuous line represents the measured velocities, the dashed-dotted line is the expected contribution from the dark halo, the short dashed line is the expected velocities based on the visible disk, and the long dashed line is the contribution from gas [1].

B. The WIMP Theory & the LZ Experiment

One of the criteria for DM candidates is that they must fit within the current measurement of the density of DM in the universe, Ω_{DM}. The current measurement includes separately the density of cold, non-baryonic matter, and that of cold, baryonic matter. Structure formation of the universe requires DM candidates to be "cold," or non-relativistic at the time of galaxy formation. They must also be stable on the lifetime of the universe, or around 10^{26} s, to have not decayed by now, and they must interact through the weak and gravitational force [2].

The current leading candidate for DM is the WIMP. WIMPs are theoretical particles in the mass range of 10 GeV - 1 TeV. WIMPs do not interact with electromagnetic waves, but experience only the weak and gravitational forces. They can self-annihilate and interact kinematically with other forces. In the expansion stage of the universe, WIMPs would have been in thermal and chemical equilibrium with Standard Model (SM) particles. However, as the universe expanded, the rate of exchange between WIMPs and SM particles would have dropped until it was less than the Hubble expansion rate of the universe. At this point, WIMP creation would have stopped and they would no longer be in thermal equilibrium. This is referred to as the WIMP "freeze out", which led to a constant WIMP density. The number of WIMPs we observe now are relics left over after the annihilation rate dropped [3].

Interestingly, particle physics independently predicts a par-

ticle with these properties, the lightest superparticle (LSP) in supersymmetric models. This coincidence, that two branches of physics independently theorized a cold, stable, and weakly interacting particle, was originally called the "WIMP miracle," and gave hope to the WIMP theory. Supersymmetry is a new theoretical symmetry of nature that predicts that every SM particle has a supersymmetric partner. To be a candidate for DM, the LSP has to be both stable and weakly interacting, which eliminates all the supersymmetric particles except the sneutrino, or supersymmetric partner of the neutrino, and the neutralino, a mix of the supersymmetric bosons. The current failure of most experiments to detect WIMPs has mostly ruled out the sneutrino as the component of DM in our galaxy, so most experiments are focusing on the neutralino as the most likely WIMP candidate [2].

The disconnect between Newtonian gravity and astrophysical observations is clear evidence that DM exists, but it has yet to be directly detected. Figure 2 represents the current and projected results of many experiments attempting to detect WIMPs. Each of the experiments sets a limit for the WIMP mass and interaction cross section. All of these efforts have set a decently narrow range of what the remaining possible mass and cross sections of this theoretical particle might be. Each collaboration, unique in their detection method and scope, has given us a good idea of what physical properties the WIMP cannot have. However, there are still models of WIMPs available, shown as shaded areas in the plot, that exist in the regions untouched by current experiments, and might be discovered by the newest generation of WIMP detectors.

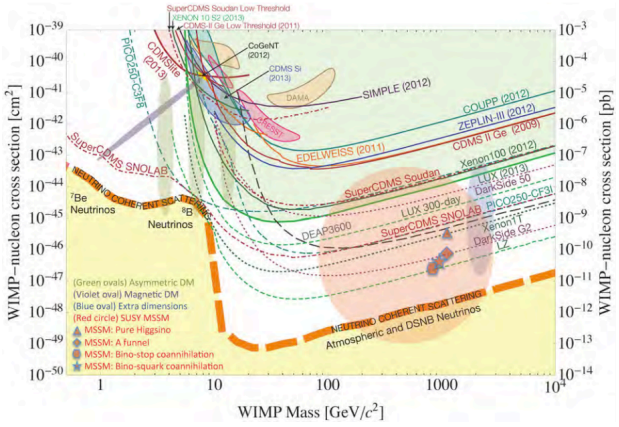

FIG. 2: WIMP mass versus cross sections showing experimental limits for past (solid curves) and future (dotted curves) detectors, as well as theoretical models (shaded regions) and the projected neutrino background [4].

One such detector is the LUX-ZEPLIN (LZ) experiment, currently in the development stage. LZ is a larger and more sensitive version of LUX, the Large Underground Xenon detector. A diagram of the detector is shown in Figure 3. With 7 tonnes of liquid xenon surrounded by layers of liquid scintillation material, water and photomultiplier tubes (PMTs), the new LZ detector will be more sensitive to an interaction, more shielded from background, and have a better ablility to reject background events [4]. The LZ detector will be built in the same lab as LUX, deep underground in the 4,850 foot level of the Sanford Underground Research Laboratory (SURF). LZ will be the most sensitive detector built, as shown in Figure 2, where it is the dark green dotted line extending furthest into the low cross-section region.

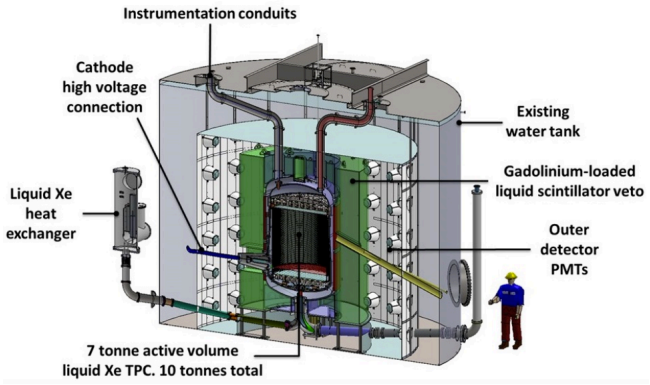

FIG. 3: A diagram of the LZ detector [4].

C. The Dark Matter Signal

LZ is a dual-phase xenon detector, which relies on nuclear recoil events to detect dark matter interactions. The center of the detector, filled with a dual layer of liquid and gaseous xenon, is known as a TPC, or Time Projection Chamber. As a particle enters the TPC, energy can be transfered to the detector in three ways: scintillation, ionization, or heat, shown in Figure 4. If the energy is lost to heat, no useable signal is created. However, if a particle interaction directly excites the xenon atoms, it produces an initial pulse of scintillation light referred to as an S1 signal. The interaction could also ionize the xenon atom, producing free electrons. These electrons could then either recombine with the surrounding xenon, adding to the scintillation (S1) signal, or they could escape. The escaped electrons are directed to the top of the detector by a strong electric field, where there is a layer of gaseous

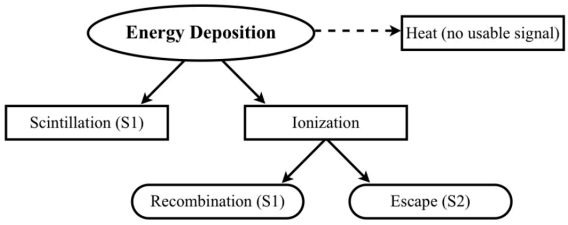

FIG. 4: The possible energy deposition of a nuclear recoil interaction in xenon. Energy can be deposited initially by creating scintillation light or by ionizing the xenon atoms. The ionized electrons can then either recombine with the xenon atom and produce additional scintillation, or escape and potentially produce an electroluminescent signal at the gaseous boundary. The final energy deposition method is through heat, which produces no usable signal [5].

xenon above the liquid layer. When the free electrons cross this boundary, they can create a secondary light signal through electroluminescence. This is called an S2 signal. By correlating the time between these two pulses, known as the drift time, and examining the geometry given by correlating signal times on adjacent PMTs, it is possible to create a three-dimensional reconstruction of the event. The TPC design of LZ is shown in Figure 5.

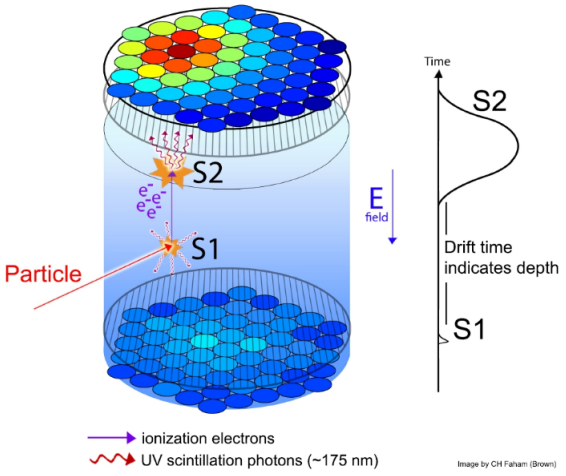

FIG. 5: Illustration of an interaction in the TPC producing a scintillation (S1) and electroluminescence (S2) signal. Correlation between adjacent PMTs allows for determination of the precise 3D location of the interaction [4]

Technical Background

D. The Davis Xenon Detector

The DAvis Xenon detector, or DAX, was built at UC Davis to be a small-scale testbed for LZ development. The detector will be used to test and improve upon instrumentation needed for the larger LZ experiment. During this summer, the DAX detector was used to test a new LZ amplifier design, a potential liquid purity monitoring system for xenon purity measurements during the experimental run, and the response of xenon to heavy element nuclear recoils using lead-206. The latter experiment is the one to which the PMT calibration was most relevant. DAX relies on a complex design incorporating vacuum spaces, nitrogen cooling systems, and liquid and gaseous xenon in the DAX TPC. There are two vacuum spaces: one to provide insulation in keeping the system cool, and the other to clear the inner chamber for insertion of xenon, maintaining its purity. The outer chamber hosts a circulation loop of nitrogen, which provides coolant to the system. The xenon in the system is recirculated through a getter which helps to remove any impurities. The inner chamber, where the TPC is housed, is cooled to about 2.6 bar and 168 Kelvin.

DAX is a dual-phase xenon TPC, like LZ, with both liquid and gaseous xenon layers. The electric field is produced by a cathode at the bottom of the TPC, a gate between the liquid and gaseous layer, and an anode at the top of the TPC. DAX relies on a single photomultiplier tube for its signal; the PMT rests on the top and looks down into the TPC. The PMT output is fed through the LZ amplifier, which has two channels. The first channel, the high gain channel, is primarily for analyzing low energy signals. In LZ, this channel is necessary for weak signals like that expected from a dark matter candidate interaction. The other channel, the low gain channel, is used for larger, more energetic pulses. This channel is more useful in detector calibration, as the signals from radioactive calibration sources are often high-energy and require much less amplification.

E. Photomultiplier Tube Calibration

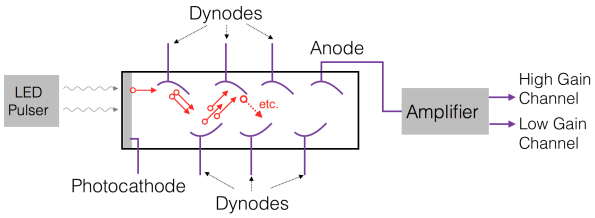

FIG. 6: Schematic of the calibration setup, including a diagram of the inside of a photomultiplier tube.

Calibration of the PMT is essential to understanding the response of the detector. In order to calibrate our PMT, we set up an LED to pulse into the inner chamber of the TPC. When an LED photon hits the photocathode of the PMT, there is some likelihood of ejecting a single photoelectron (PE). That PE is then focused onto the first dynode in the chain of the PMT (see Figure 6). Each successive dynode is held at a higher potential, so that once an electron strikes the first dynode, it will cascade down the chain. At each dynode, more electrons are produced, exponentially increasing the number of electrons collected at the anode. The gain of the PMT is the ratio of the number of electrons incident on the anode to the number generated at the photocathode. The amplified pulse produced at the anode is then sent into the LZ amplifier, where it is split into both the high and low gain channel. The goal of the measurement is the pulse area that, after the signal chain of both the PMT and amplifier, corresponds to a single electron released from the photocathode.

In order to ensure that the gain we measure is due to that of a single PE, the LED pulse width and voltage was set such that only approximately 10% of the PMT triggered events showed a PE event. Allowing only a low light density into the TPC chamber ensures that the majority of events will be due to a single PE, with a small percent of multiple PE events as well as events with only noise. The data acquisition software in place is able to distinguish between PE events and noise-only events and automatically calculate the PE pulse area. The analysis first uses baseline integration to find the noise level of the data. It then looks for any pulse above a certain thresh-

old, readjusting for baseline as it moves along. The program automatically filters and classifies the pulses as S1 or S2. The beginning of the summer was spent adjusting the parameters of this program, and implementing a more accurate method of calculating baseline, which greatly improved the pulse classification efficiency. In the PMT calibration, the TPC is not filled. The pulses appear as S1 signals, since they are narrow pulses, though they are produced by the LED and not by scintillation light.

With each pulse, the pulse area is calculated automatically by subtracting the baseline from each sample, removing the DC offset. Then the algorithm loops through each sample in the region classified as the pulse and calculates the total area. The total pulse area is then plotted as a histogram for a range of bias voltages on the PMT. The data at 800 V in the low gain channel is shown in Figure 7. The same data was taken for PMT bias voltages at 700, 750, 800, and 900 V, and the histograms were made in both the high and low gain channels.

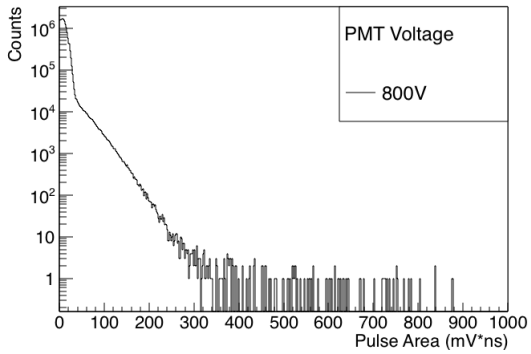

FIG. 7: Histogram of the pulse areas measured with 800 V supplied to the base of the PMT in the low gain channel.

Results & Discussion

The experimental goal was to find the mean of the single photoelectron population. In Figure 7, the peak centered around zero is due to baseline noise integration, and is called the noise pedestal. The shoulder of the pedestal is the single PE population. In the data, it is evident that the expected peak due to the single PE was non-negligibly close to the noise pedestal. There is some debate over the best theoretical distribution to use when fitting to a PMT distribution. Previous work by a member of the group showed that when compared to a continuous Poisson fit and a standard Gaussian, a truncated Gaussian outperformed the other two and has additional benefits when the single PE peak is non-negligibly close to the noise pedestal, as in our data [6].

Because the single PE peak is so close to the noise pedestal, in a simple Gaussian fit to the peak, the mean of the Gaussian results in a negative pulse area. Since the pulse area is by definition a positive quantity, the negative pulse area is a non-physical result. Instead, the data was fit to a truncated Gaussian, which takes only into account the positive, or physical, pulse areas. The truncated Gaussian is given by the function

$$T(H, \mu, \sigma; x) = \Theta(x) H e^{-(x-\mu)^2/\sigma^2} \quad (1)$$

where $\Theta(x)$ is the Heaviside step function, which defines the function to be zero when x is negative, effectively cutting out any negative pulse areas.

In order to fit the data to a truncated Gaussian, we first fit both the noise pedestal and the shoulder to separate Gaussian functions and then combined the parameters into a single fit over the entire distribution, as shown in Figure 8. The parameters of the combined fit were then passed to the truncated Gaussian function, and the mean and standard deviation calculated from standard methods. This process was repeated for four PMT bias voltages in both the high and the low gain channels. Each distribution and the combined fit in the high gain channel is shown in Figure 9.

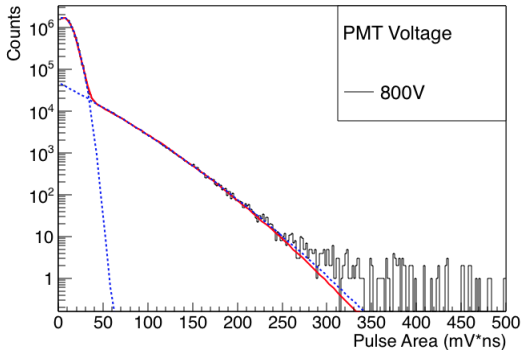

FIG. 8: Gaussians are fit to both the noise pedestal and single PE distribution (blue dotted lines) and the parameters passed to a combined Gaussian fit over the whole distribution, shown in red. This is the low gain channel with an 800 V PMT bias.

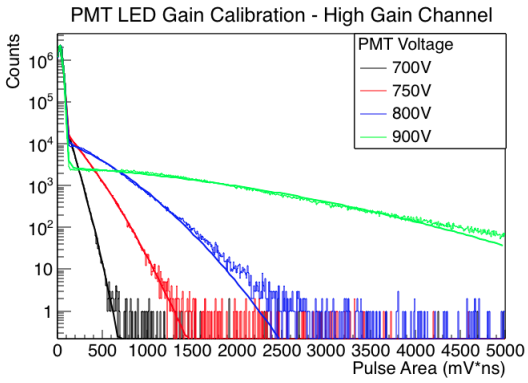

FIG. 9: The combined fit for each of the four PMT bias voltages, shown in the high gain channel .

The mean of the truncated Gaussian corresponds to the mean area of the pulse produced from a single PE, in units of millivolt nanoseconds, or mV·ns. For both the high and low gain channels, the gain of a PMT increases exponentially with bias voltage, as our data shows in Figure E. The error

on each mean, accounting for systematic and statistical errors, are on average a few percent and are too small to be visible on the plot.

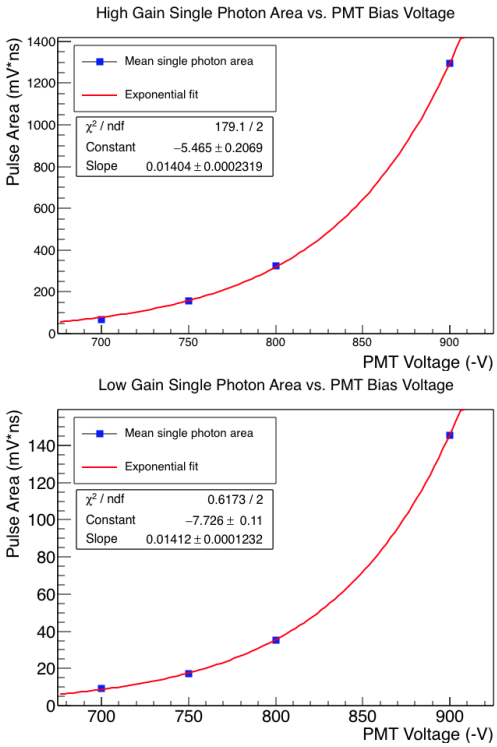

FIG. 10: Single photon area versus applied PMT voltage, with PMT gain fit by an exponential function for both the high gain and low gain channels.

Knowing the single photon area of the PMT at each bias voltage informs the optimal setting of the PMT in future work. The optimal setting balances both resolution and gain. The resolution of the PMT defined as the ratio of the single PE pulse width to its area. The width is given by σ of the truncated Gaussian. A plot of the PMT resolution as a function of bias voltage is shown in Figure 11. The PMT resolution is above 80% for all bias voltages, and the voltage with the highest gain is 900 V in both channels. However, the 900 V setting also has the lowest resolution, below 90% for both high and low gain. We decided to select 800 V as the operating bias voltage in future experiments with DAX, as it had the next highest gain with a resolution of 87% in the low gain channel and 92% in the high gain channel.

Another interesting verification of the LZ amplifier is the difference in gain between the two channels. At 800V, the single photon area of the high gain channel is 325.26 mV·ns, and for the high gain channel it is 35.34 mV·ns. The factor difference in the two channels is 9.2. The ratio for each voltage is shown in Table I. The expected gain difference between the two channels is a factor of 10, and each of the ratios is within operational limits. The difference is closest to 10 for our chosen bias voltage, 800 V.

Finding the optimum setting for our PMT in terms of gain and resolution, and finding the single photoelectron area were

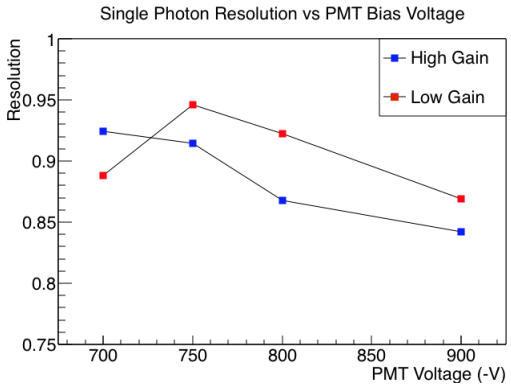

FIG. 11: PMT resolution, defined as mean single photon pulse width over area, for each bias voltage.

Bias Voltage	Ratio of HG/LG Area
700	7.14
750	9.04
800	9.20
900	8.89

TABLE I: Ratio of single photon area of the high gain channel to that of the low gain channel.

major accomplishments which furthered the scientific goals of DAX. With this number, pulse dimensions can be converted from mV·ns to a more versatile unit, photoelectrons (phe), by dividing each pulse area by the single photoelectron area. By doing this, the size of any pulse can be measured in how many photoelectrons were produced, making the result independent of the PMT gain and a better measure of how energetic the pulse was.

Conclusion & Further Work

Understanding the function of the PMT is an essential beginning to a full calibration of DAX. This project calibrated the PMT, resulting in the optimal bias voltage and the single photoelectron area at that bias voltage, which will aid future research with the system. An additional contribution of this summer's work was an improved pulse finder algorithm that can more accurately distinguish between S1 and S2 pulses.

After the conclusion of the PMT calibration, the focus turned towards energy calibration of DAX. We placed radioactive sources with well-known energy spectra adjacent to the TPC, and measure the area of the S1 and S2 pulses produced within the detector. This gives a spectrum in pulse area that is easily matched to the known energy spectrum of the calibration source, allowing for precise correlation of the response of the detector to an energy scale. Unfortunately, timing difficulties associated with cooling down and filling the TPC with xenon allowed us to only take a few calibration runs before the end of the summer. With very little data, no conclusions could be drawn. However, energy calibration is an ongoing

project of the LZ team at Davis. With this and future work, the contributions of this summer have helped pave the way for a fully calibrated DAX and future testing of the mechanisms of dark matter interactions.

Acknowledgements

This project was completed in collaboration with Jacob Cutter and Tyler Anderson. I would like to thank them for their tremendous help and support, especially in development of the software. I would also like to thank Dr. Mani Tripathi, the project advisor, for the opportunity and guidance. Thanks also to Rena Zieve and the UC Davis REU program for providing an incredible learning experience. Finally, thank you to the NSF for funding this program.

[1] E. Corbelli and P. Salucci, Monthly Notices of the Royal Astronomical Society **311**, 441 (2008), 9909252v1.

[2] Patrignani, et al. (Particle Data Group), Chin. Phys. C **40** (2016).

[3] G. Bertone, D. Hooper, and J. Silk, Physics Reports **405**, 279 (2004), 0404175v2.

[4] Harris, A., et al., The LUX-ZEPLIN (LZ) Collaboration, *LUX-ZEPLIN (LZ) Conceptual Design Report* (2015).

[5] M. Szydagis, N. Barry, K. Kazkaz, J. Mock, D. Stolp, M. Sweany, M. Tripathi, S. Uvarov, N. Walsh, and M. Woods, Journal of Instrumentation **6** (2011), arXiv:1106.1613v1, URL `https://arxiv.org/pdf/1106.1613.pdf`.

[6] A. O. Manalaysay, Ph.D. thesis, University of Florida (2009).